

Structural Properties of Ruthenium Biimidazole Complexes Determining the Stability of their Supramolecular Aggregates

Nils Rockstroh^{a,b}, Katrin Peuntinger^{a,c}, Helmar Görls^b, Dirk M. Guldi^c, Frank W. Heinemann^a, Bernhard Schäfer^b, and Sven Rau^{a,b}

^a Department for Chemistry and Pharmacy, Friedrich-Alexander-Universität Erlangen-Nürnberg, Egerlandstraße 1, 91058 Erlangen, Germany

^b Institut für Anorganische und Analytische Chemie, Friedrich-Schiller-Universität Jena, August-Bebel-Straße 2, 07743 Jena, Germany

^c Department for Chemistry and Pharmacy & Interdisciplinary Center of Molecular Materials (ICMM), Friedrich-Alexander-Universität Erlangen-Nürnberg, Egerlandstraße 3, 91058 Erlangen, Germany

Reprint requests to Prof. Dr. Sven Rau. E-mail: sven.rau@chemie.uni-erlangen.de

Z. Naturforsch. **2010**, *65b*, 281–290; received January 12, 2010

Dedicated to Professor Rolf W. Saalfrank on the occasion of his 70th birthday

The results of a detailed investigation of the influence of substituents in a variety of ruthenium biimidazole-type complexes $[\text{Ru}(\text{R-bpy})_2(\text{R}'\text{-bi}(\text{bz})\text{imH}_2)]^{2+}$ ($\text{R} = \text{H}, \text{'Bu}$; $\text{R}' = \text{H}, \text{Me}$; $\text{bi}(\text{bz})\text{imH}_2 = 2,2'\text{-bi}(\text{benz})\text{imidazole}$) on selected structural and photophysical properties is reported. The photophysical properties are only marginally influenced by the substituents at the bipyridine and the biimidazole core. All complexes show intense absorptions in the visible range of the spectrum with maxima around 475 nm, and emission from the formed excited state occurs at wavelengths between 650 and 670 nm. The comparison of structural properties determined by X-ray analysis within a series of related complexes shows that the Ru–N bond lengths to the coordinated bipyridines are not significantly influenced by the substituents, but slight differences in the Ru–N bond lengths to the biimidazole-type ligands can be detected. The reactions between ruthenium complexes containing different biimidazole-type ligands with the sulfate dianion, however, show a strong correlation between the substituents at the biimidazole core and the solubility of the product. The bibenzimidazole-containing complexes precipitate from aqueous solution whereas the ruthenium complex containing unsubstituted biimidazole stays in solution. The solid-state structure of one example of the sulfate-containing products (**2b**) shows that strong hydrogen bonds between the secondary amine function of the bibenzimidazole and the oxygen functionalities of the sulfate contribute to this unexpected behavior.

Key words: Ruthenium, Biimidazole, Bibenzimidazole, Supramolecular Chemistry, Hydrogen Bonds

Introduction

Ruthenium polypyridyl complexes have attracted much attention during the last decades due to their exceptional photochemical and photophysical properties [1]. These complexes are able to bind a broad variety of chelating ligands to form mononuclear complexes as well as complexes of higher nuclearity depending on the choice of the ligand [2–5]. These assemblies are supposed to act as artificial systems for photosynthesis. It is well known that hydrogen bonds play an important role in the naturally occurring process. Therefore, the use of ligands which are able to act as hydrogen bond donors and acceptors is a promising way to

mimic this system. Possible candidates are complexes of ruthenium bearing NH-functionalized ligands, *e. g.* biimidazole or bibenzimidazole. These complexes allow the interaction with several monoanions in organic solvents [6–8]. For instance, a dicationic ruthenium bibenzimidazole complex can act as an active hydrogen bond donor, while the acceptor is a monocationic osmium bipyridine carboxylate [8]. This association allows efficient energy transfer from the ruthenium to the osmium moiety in accord with proposed requirements in photosynthetic processes. Efficiency and directionality of energy and electron transfer processes strongly depend on this kind of supramolecular forces. The complexes are promising candidates for

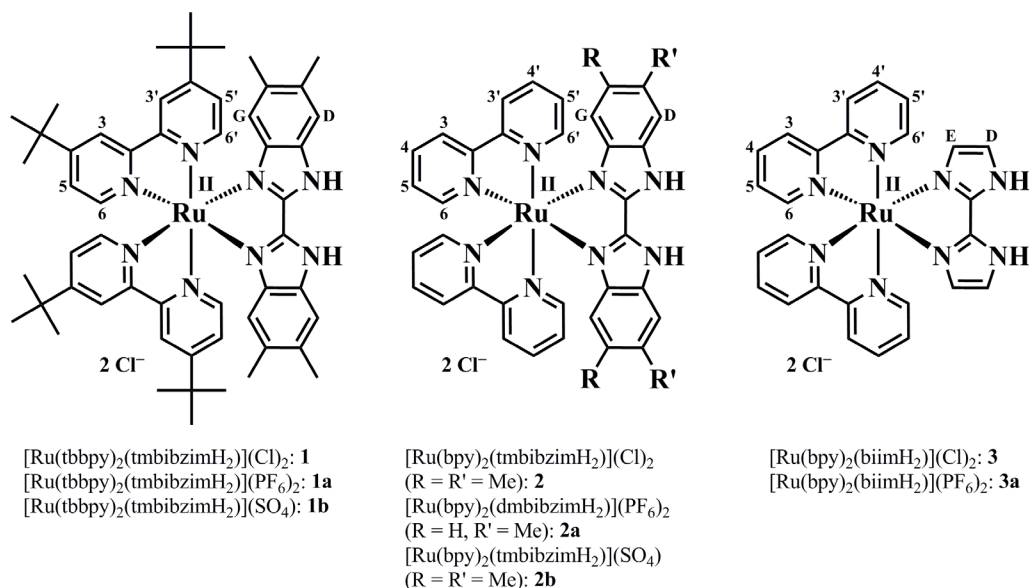


Fig. 1. Chemical structures of investigated compounds **1**, **1a**, **1b**, **2**, **2a**, **2b**, **3** and **3a**.

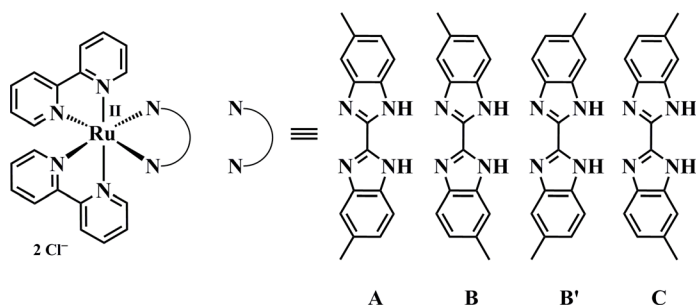


Fig. 2. Three possible isomers of the dimethyl-benzimidazole ligand coordinated in **2a**. Note that B and B' are equivalent and therefore occur twice as often as A or C.

multistep catalytic processes within biomimetic systems. Furthermore, modifications with special hydrogen bond acceptors like perfluorooctylcarboxylate lead to a change in chemical properties. So, the complex [Ru(tbbpy)₂(bibzimH₂)](Cl)₂ becomes soluble in supercritical carbon dioxide upon the addition of perfluorooctylcarboxylate [7]. Ye and coworkers have confirmed the capability of biimidazole complexes to act as hydrogen bond donors by means of NMR and UV/Vis spectroscopy [6]. It could be shown that the complex [Ru(bpy)₂(bibzimH₂)](PF₆)₂ acts as hydrogen bond donor towards several monoanionic ions like Cl⁻, Br⁻, I⁻, NO₃⁻, HSO₄⁻, H₂PO₄⁻, OAc⁻, and F⁻. All these investigations comprise the interaction of monoanions with the NH functions of these complexes in organic solvents. To the best of our knowledge, these assemblies are unstable in aqueous solution which represents a serious draw-

back for their future application. Hence, it is necessary to develop an understanding of how to influence the stability of aggregates in solution by steric and/or electronic tuning of host molecules as well as their guests. Herein, we report on the interaction of the sulfate dianion with the ruthenium bibenzimidazole complexes [Ru(tbbpy)₂(tmbibzimH₂)](Cl)₂ (**1**) and [Ru(bpy)₂(tmbibzimH₂)](Cl)₂ (**2**), and the biimidazole complex [Ru(bpy)₂(biimH₂)](Cl)₂ (**3**) (Fig. 1) in water, which show unexpected differences.

Results and Discussion

Synthesis and characterization

The compounds **1**, **2** and **3** were prepared using literature methods [9, 10]. The ¹H-NMR spectra of **1** and **2** show the typical signals for octahedral ruthenium(II) bipyridine complexes containing bibenzimidazole. The

Table 1. UV/Vis and emission data of **1–3** in water and excited state lifetimes in aerated water at room temperature.^a

| Complex | $\lambda_{\max, \text{abs}}$ (nm) | ϵ_{MLCT} (L mol ⁻¹ cm ⁻¹) | Emission (nm) | Lifetime τ (ns) |
|----------|-----------------------------------|---|------------------|-------------------------|
| 1 | 292, 347, 366, 482 | 8400 | 668 | 219 |
| 2 | 289, 342, 361, 472 | 9300 | 654 | 95 |
| 3 | 289, 340, 477 | 9000 | 650 | ^b |

^a **2b** has not been investigated in detail as no pure isomer could be isolated; ^b not determined.

singlets for the phenylene groups in the tetramethylbibenzimidazole ligand show no differences between **1** and **2** ($\delta(\text{H}_G) = 7.48$ ppm, $\delta(\text{H}_D) = 5.35$ ppm). On the other hand, the bipyridine signals differ slightly due to the steric and electronic influence of the *tert*-butyl groups. Thus, signals 3 and 3' of **1** are shifted to lower field by approximately 0.35 ppm compared to **2**. Additionally, signals 6 and 6' of **1** are down-field shifted by more than 0.1 ppm. Signals 5 and 5' show no significant differences upon substitution of H by *tert*-butyl groups in 4 and 4' position. Compound **3** exhibits a similar set of signals just differing in the shielding of the biimidazole protons, which appear as two doublets at 7.26 and 6.38 ppm. ¹H-NMR investigations of **2a** have identified a statistical mixture of three possible isomers in a 1 : 2 : 1 ratio (Fig. 2). The ratio of signal integrals of the methyl groups compared with those of the arene signals prove the stoichiometry of **2a**.

Absorption and emission spectra

The UV/Vis absorption and emission data of **1–3** in water are presented in Table 1. The absorption spectra exhibit a UV transition at approximately 290 nm indicative of intraligand π - π^* transitions of the bipyridine ligands. The absorptions at about 345 and 365 nm can be assigned to intraligand π - π^* transitions of the biimidazole type ligands. Furthermore, in **3** only one transition within this region can be observed at 340 nm. Thus, the transition at about 365 nm is characteristic of the anellated phenyl rings of the bibenzimidazole ligand. All complexes show the characteristic ¹MLCT absorption band at approximately 475 nm. For **1**, only a small influence of the solvent on the absorption properties is observed. Thus, the absorption maximum of **1a** in acetonitrile at 480 nm [11] is not significantly different from that of **1** in water (482 nm). Furthermore, comparison of **1** and **2** shows that the *tert*-butyl groups of **1** cause a bathochromic shift of the ¹MLCT transition by 10 nm. This shift is most likely caused by the electron donating effect of the

tert-butyl σ donor) which increases the electron density of the metal center lowering the excitation energy of the metal to ligand charge transfer transition. A similar bathochromic shift could be observed if the bibenzimidazole is replaced by the biimidazole ligand (compare Table 1). Thus, biimidazole appears to be a stronger π donor than bibenzimidazole [10]. Additionally, in the emission spectra a significant red shift from 654 (**2**) to 668 nm (**1**) reveals the stronger σ -donating effect of the *tert*-butylbipyridine compared to the bipyridine group. The reason for this observation is the somewhat higher level of the highest occupied *d* orbital at the metal center and therefore a smaller energy gap between this orbital and the π^* orbital of the *tert*-butylbipyridine. Consequently, there is no significant difference between the emission wavelengths of **2** and **3**. Comparison of lifetimes of the excited states of **1** and **2** show that the sterically more demanding *tert*-butyl groups present in **1** result in longer lifetimes compared with lifetimes obtained for **2** containing unsubstituted bipyridines. A possible explanation for this observation can be found in the weaker interaction of the polar solvent water with the sterically protected bipyridine ligands. It should be noted that **1a** exhibits a similar lifetime in deaerated acetonitrile (260 ns) as **1** in aerated water (219 ns) [11]. This effect could either be explained by the prolongation of the excited state lifetime in protic solvents like water, or by the assumption that the excited state formed is not quenched by oxygen in water to a large extent. The latter is rather unlikely as the lifetime of the excited state of ruthenium complexes is normally quenched by 30 % by oxygen in aqueous solution [12].

Solid-state structural characterization

A few examples of tetramethylbibenzimidazole complexes and their structural characterization have been described in the literature [7, 13, 14]. A structural motif was published for **1a** several years ago [11] suggesting the formation of **1a**. We were now able to obtain crystals of higher quality so that structural properties of **1a** could be analyzed. The molecular structures of **1a**, **2a** and **2b** and the corresponding bond lengths and angles are shown in Figs. 4, 5 and 6, respectively, and in Table 2. The numbering scheme used in Table 2 is depicted in Fig. 3.

The ruthenium atom has a distorted octahedral environment. The distances between the bibenzimidazole nitrogen atoms and the metal (2.110(4) and 2.102(5) Å) are longer than those between the

Table 2. Selected bond lengths (Å) and angles (deg) of **1a**, **2a** and **2b**. The numbering scheme is according to that depicted in Fig. 3.

| | 1a | 2a | 2b |
|--|------------|------------|-----------|
| Ru1–N1 | 2.110(4) | 2.084(3) | 2.080(8) |
| Ru1–N2 | 2.102(5) | 2.084(3) | 2.084(7) |
| Ru1–N5 | 2.042(4) | 2.038(3) | 2.034(9) |
| Ru1–N6 | 2.053(5) | 2.059(3) | 2.052(7) |
| Ru1–N7 | 2.058(4) | 2.059(3) | 2.055(7) |
| Ru1–N8 | 2.059(4) | 2.038(3) | 2.039(9) |
| C7–C8 | 1.424(7) | 1.445(11) | 1.406(12) |
| N5–Ru1–N6 | 79.01(18) | 78.71(12) | 79.5(3) |
| N5–Ru1–N7 | 95.81(18) | 97.64(12) | 93.9(3) |
| N6–Ru1–N7 | 172.15(18) | 175.03(18) | 171.7(3) |
| N5–Ru1–N8 | 95.54(17) | 87.10(17) | 89.0(4) |
| N6–Ru1–N8 | 95.60(17) | 97.64(12) | 95.0(3) |
| N7–Ru1–N8 | 78.93(17) | 78.71(12) | 79.8(3) |
| N5–Ru1–N2 | 94.24(18) | 97.61(14) | 96.0(3) |
| N6–Ru1–N2 | 93.07(18) | 86.65(13) | 91.0(3) |
| N7–Ru1–N2 | 93.19(18) | 97.23(13) | 94.7(3) |
| N8–Ru1–N2 | 168.00(17) | 174.20(13) | 172.8(3) |
| N5–Ru1–N1 | 171.20(18) | 174.20(13) | 173.1(3) |
| N6–Ru1–N1 | 97.79(18) | 97.23(13) | 97.7(3) |
| N7–Ru1–N1 | 88.17(17) | 86.65(13) | 89.4(3) |
| N8–Ru1–N1 | 92.92(17) | 97.61(14) | 97.5(4) |
| N2–Ru1–N1 | 77.66(17) | 77.9(2) | 77.7(3) |
| N1–C7–C8 | 117.4(5) | 116.2(3) | 115.6(8) |
| N3–C7–C8 | 129.7(5) | 132.0(3) | 131.6(9) |
| N2–C8–C7 | 116.8(5) | 116.2(3) | 117.7(7) |
| N4–C8–C7 | 130.3(5) | 132.0(3) | 130.4(8) |
| N1–C7–C8–N2 | –0.1(8) | –0.8(7) | –2.6(11) |
| Bending angle of tmbibzimH ₂ ^a | 167.1 | 164.2 | 165.7 |

^a The angle between two lines constructed from the centroid of the benzene ring of one half of the ligand and the corresponding bridging atom as used in ref. [14].

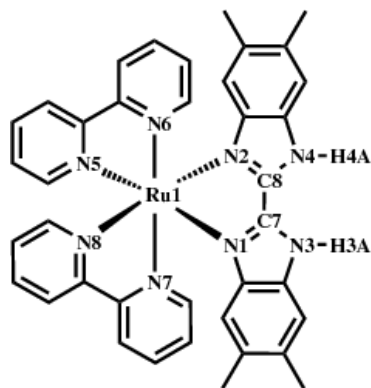


Fig. 3. Numbering scheme for the comparison of the structural parameters of **1a**, **2a** and **2b** in Table 2.

ruthenium and the tbbpy nitrogen atoms (2.042(4)–2.059(4) Å) showing a weaker binding of the former. This is in good agreement with the results published for [Ru(tbbpy)₂(bibzimH₂)](Cl)₂, where the methyl groups of the tetramethylbibenzimidazole ligand are

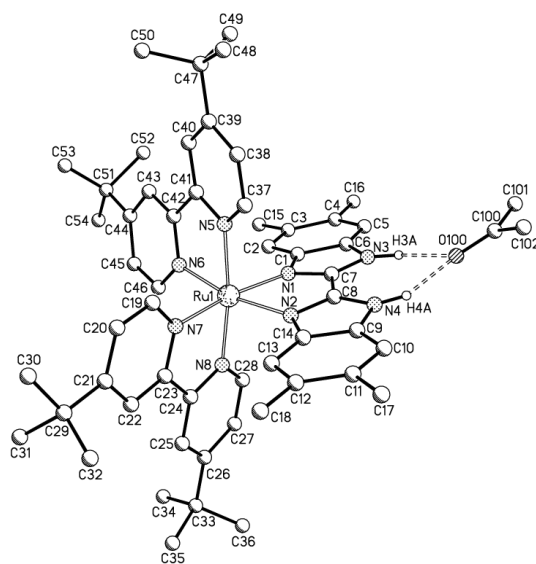


Fig. 4. Solid-state molecular structure of the dication of **1a**. Counterions, solvent molecules except for the hydrogen-bonded acetone and hydrogen atoms except for the NH protons are omitted for clarity.

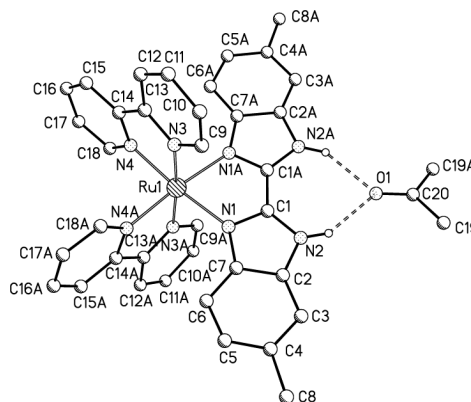


Fig. 5. Solid-state molecular structure of the dication solvate of **2a**. Shown is the isomer with both methyl groups directed away from the ruthenium center. Hydrogen atoms except for the NH protons, counterions and solvent molecules except for the hydrogen-bonded acetone are omitted for clarity.

replaced by hydrogen atoms [14, 15]. In compounds **2a** and **2b**, where the tbbpy ligands are replaced by bpy ligands, the linkage of these ligands to the ruthenium center shows no significant difference from that in **1a**. On the other hand, the bibenzimidazole ligands in **2a** and **2b** have a slightly shorter distance to the metal than in **1a**, owing to the electronic effect of the tbbpy ligands in **1a**. In all compounds containing bibenzimidazole as ligand, a bent arrangement of the bibenzimidazole around the metal ion could be observed. Thus in

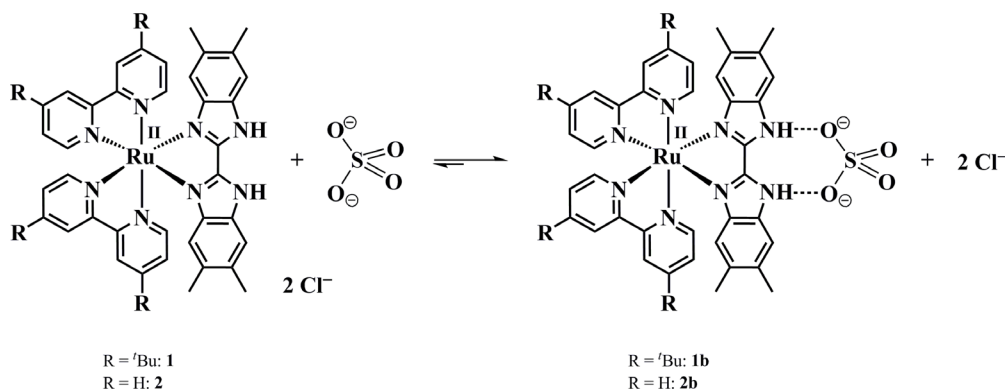


Fig. 7. Tight ion binding through hydrogen bonds between the cations in **1** and **2** and sulfate.

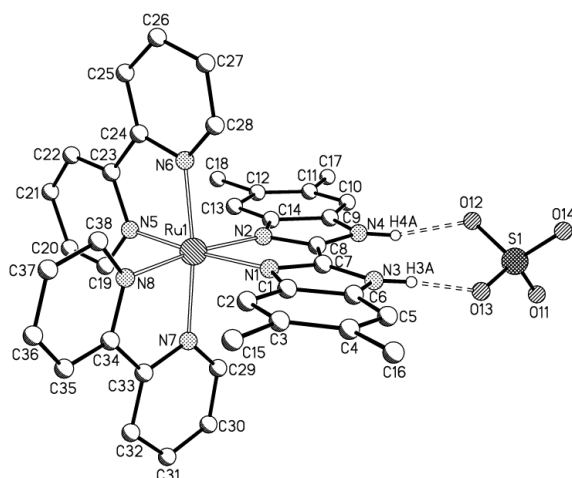


Fig. 6. Solid-state molecular structure of **2b**. Solvent molecules and hydrogen atoms except for the NH protons are omitted for clarity.

1a, **2a** and **2b**, the angles $\angle \text{N1-C7-C8}$ and $\angle \text{N2-C8-C7}$ are smaller than 120° , while the angles $\angle \text{N3-C7-C8}$ and $\angle \text{N4-C8-C7}$ exceed 120° . This is also similar to the molecule $[\text{Ru}(\text{tbbpy})_2(\text{bibzimH}_2)](\text{Cl})_2$, where the bending angle of bibzimH_2 , which is defined as the angle between two lines constructed from the centroid of the benzene ring of one half of the ligand and the corresponding bridging atom, has a value of 166.3° [14]. The bending angles of **1a** (167.1°), **2a** (164.2°) and **2b** (165.7°) are within the same range. The structure of **3** is disordered and is therefore not presented. To solve this structure, several assumptions and calculations had to be made so that no differences between the Ru–N distances and the resulting angles could be specified. However, mass spectrometry of the single crystals measured on the diffractometer revealed that the crystal contained exclusively **3**.

The NH functions of compounds **1** and **2** act as hydrogen bond donors in the presence of suitable hydrogen bond acceptors like solvent molecules or anionic species [6, 8, 11]. The two compounds show good solubility in water. Upon the addition of very small amounts of sulfate, **1** and **2** form precipitates, while **3** stays in solution (Fig. 7).

The addition of 0.15 mL of a 3.3×10^{-3} M aqueous solution of sodium sulfate to 100 mL of a 2.2×10^{-4} M solution of **2** in water leads to a precipitation of **2b**, corresponding to a $K_L < 1.1 \times 10^{-9} \text{ mol}^2 \text{ L}^{-2}$. The consideration of $\text{p}K_a$ values can provide a first explanation for this unexpected behavior. Thus, $\text{p}K_a$ values of the complex $[\text{Ru}(\text{bpy})_2(\text{bibzimH}_2)]^{2+}$ ($\text{p}K_{a1} = 5.74$, $\text{p}K_{a2} = 10.51$) are lower than those of the complex $[\text{Ru}(\text{bpy})_2(\text{biimH}_2)]^{2+}$ ($\text{p}K_{a1} = 7.2$, $\text{p}K_{a2} = 12.1$) indicating a better hydrogen donicity of the former [16, 17]. Furthermore, this unexpected behavior could be elucidated by crystal structure investigations of **2b** (Fig. 6). The sulfate ion is linked directly to the NH functions through hydrogen bonds. According to the literature, shorter distances N–H and H \cdots O cause a stronger repulsion force between N and O and, therefore, the N–H \cdots O angle increases with increasing hydrogen bond attraction [18]. Consequently, a strong hydrogen bond is correlated to a larger D–H \cdots A angle and shorter distances between the involved atoms [18]. The hydrogen bonds in **2b** are quite strong as it can be deduced from the distances and N–H \cdots O angles depicted in Table 3.

In compound **1a** the N–H \cdots O angle (O from acetone) is approximately 150° , therefore the distances between H and O (2.11 and 2.00 Å, respectively) are larger than in **2b** (1.868 and 1.820 Å, respectively) where the N–H \cdots O angle (O from sulfate) is larger (approximately 165°). The comparison of van

Table 3. Selected hydrogen bond lengths (Å) and angles (deg) of **1a**, **2a**, and **2b**^a.

| D–H···A | D–H | H···A | D···A | ∠D–H···A |
|------------|------|-------|----------|----------|
| 1a | | | | |
| N3–H3A–O | 0.88 | 2.11 | 2.892(7) | 148.0 |
| N4–H4A–O | 0.88 | 2.00 | 2.808(7) | 151.3 |
| 2a | | | | |
| N3–H3A–O | 0.86 | 2.06 | 2.90(2) | 173.0 |
| N4–H4A–O | 0.86 | 2.06 | 2.90(2) | 172.9 |
| 2b | | | | |
| N3–H3A–O13 | 0.86 | 1.87 | 2.69(2) | 166.87 |
| N4–H4A–O12 | 0.86 | 1.82 | 2.65(2) | 163.04 |

^a D: donor atom (N); A: acceptor atom (O), interaction with acetone (**1a** and **2a**) and sulfate (**2b**), respectively.

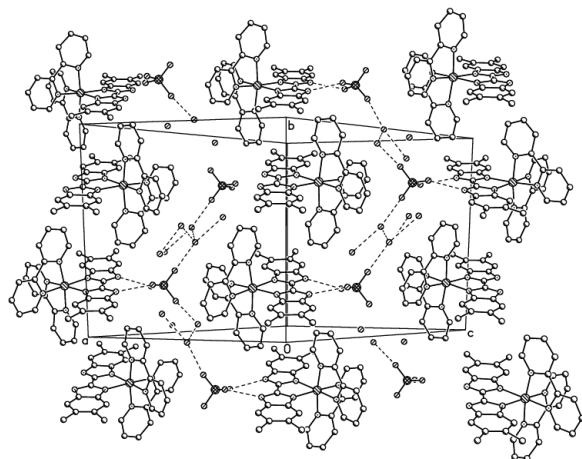


Fig. 8. Crystal structure of **2b** viewed along [101]. Hydrogen atoms are omitted for clarity.

der Waals radii confirmed our conclusions regarding the strong hydrogen bonds in **2b** [19]. The van der Waals radii of H, N and O are 1.06, 1.46 and 1.42 Å, respectively. The sum of the radii of N and O (2.88 Å) is larger than the observed lengths in **2b** (2.713 and 2.654 Å, respectively). Similar results could be obtained for the H···O bonds: The sum of the van der Waals radii of H and O is larger (2.48 Å) than found for the H···O bonds (1.868 and 1.820 Å, respectively). **2a** shows a similar hydrogen bond behavior towards acetone like **1a**. All relevant distances are in the same range. However, the correlation between angle and hydrogen bond strength could not be observed in this case.

The addition of sulfate ions to a solution of [Ru(bpy)₂(tmbibzimH₂)](Cl)₂ (**2**) in water leads to the formation of the highly ordered crystalline structure of **2b** depicted in Fig. 8.

The sulfate ions bind to the hydrophilic positions of the complex through strong hydrogen bonds.

Hence, they provide a directionality in the resulting supramolecular network. Because of this binding two different types of layers can be observed. The lipophilic ones are proposed to be responsible for the poor solubility in water and the hydrophilic ones arise from the hydrogen bond interaction of the sulfate ions with the surrounding water molecules. Another reason for the arrangement of the components in two separate layers is the linkage of sulfate ions to water molecules and not to the bibenzimidazole moiety of another dication. This may be due to the tetrahedral geometry of the sulfate ions. A hydrogen bond formation to a second cation of **2b** would lead to a right-angled assembly of the molecules which might result in a less close and therefore unfavorable packing in the crystal.

Conclusion

In this paper, the influence of different substituents in ruthenium complexes bearing biimidazole-type ligands with respect to the photophysical and structural properties was investigated. Absorption and emission properties of the complexes **1**, **2** and **3** are quite similar in aerated water. All complexes show the characteristic ¹MLCT absorption band in the visible range of the spectrum at approximately 475 nm. All compounds emit at wavelengths between 650 and 670 nm. The lifetime of the excited states of **1** and **2** (219 and 95 ns, respectively) in the presence of oxygen in aqueous solution are relatively long in comparison to related ruthenium complexes in the absence of oxygen [11]. X-Ray structure determinations on selected complexes were performed. The Ru–N bond lengths to the coordinated bipyridines are not significantly influenced by the substituents of the bipyridine ligands. However, the Ru–N bond lengths to the coordinated biimidazole-type ligands are significantly longer than those to the bipyridines revealing a stronger binding to the ruthenium of the latter. The reaction between ruthenium complexes containing different biimidazole-type ligands with the sulfate dianion in water results for **1** and **2** in the formation of insoluble compounds **1b** and **2b**, while **3** stays in solution. Preliminary investigations have shown that precipitation occurs already at concentrations as low as $4.9 \times 10^{-6} \text{ mol L}^{-1}$ for sulfate, corresponding to a solubility constant of $K_L < 1.1 \times 10^{-9} \text{ mol}^2 \text{ L}^{-2}$. Due to the quantitative precipitation of **1b** and **2b** no conductivity measurements could be performed. Based on X-ray investigations of the precipitated **2b**, we could show for the first time

that the dication of **2** acts as hydrogen bond donor with doubly charged anions like sulfate. The resulting hydrogen bonds are very strong as concluded from hydrogen bond lengths and angles. This exceptionally high stability is in contrast to previous observations with other hydrogen bond acceptors like F^- , Cl^- , $R-COO^-$ which also show an interaction with ruthenium bibenzimidazole complexes, but no formation of extended aggregates [6, 7, 14]. Based on the strong hydrogen bond interaction between the ruthenium complex and the sulfate dianion which has been structurally characterized here for the first time, construction of more elaborate light-harvesting centers in aqueous solution based on supramolecular interactions seems feasible. The influence of the peripheral substituents of the biimidazole core on the stability of hydrogen bonded aggregates will be subject of further investigations which are aimed at establishing robust supramolecular homogeneous systems.

Experimental Section

UV/Vis spectra were obtained using a Perkin Elmer Lambda2 spectrometer with a width of slit of 2 nm and a scan rate of 480 nm min^{-1} . Emission spectra were recorded using a Jasco FP-6200 spectrofluorometer and a Jobin Yvon Horiba FluoroMax-3 spectrometer with a width of the excitation and emission slit of 2 nm and an integration time of 0.5 s. Lifetime measurements were obtained using a Jobin Yvon Horiba FluoroLog3 time-correlated single-photon-counting apparatus (TCSPC). Excitation occurred with a nanoLED of 467 nm, maximum of repetition rate 250 kHz, width of pulse ≤ 200 ps, detection: Hamamatsu MCP photomultiplier (model R3809U-50, counts: 5000). The NMR spectra were recorded on Bruker (400 MHz/200 MHz) and Jeol EX-270 DELTA spectrometers (270 MHz). The mass spectra were recorded with a SSQ 710 spectrometer (Finnigan MAT). Electrospray ionization spectra were recorded with a MAT 95 XL instrument (Thermoquest-Finnigan MAT).

X-Ray crystallography: Intensities for the X-ray crystal structure determinations were collected on two different instruments: Diffraction data for crystals of **1a** and **2b** were collected at 150 K on a Bruker-Nonius Kappa CCD diffractometer, for crystals of **2a** and **3a** at 183 K on a Nonius Kappa CCD diffractometer, with graphite-monochromatized $MoK\alpha$ radiation ($\lambda = 0.71073$ Å). Data were corrected for Lorentz and polarization effects. Additionally, for compounds **1a** and **2b** semiempirical absorption corrections were performed on the basis of multiple scans using SADABS [20], but not for **2a** and **3a** [21, 22]. The structures of **1a** and **2b** were solved by Direct Methods and refined by full-matrix least-squares procedures on F_o^2 using SHELXTL NT (v6.12) [23], while

the structures of **2a** and **3a** were solved by Direct Methods using SHELXS [24] and refined by full-matrix least-squares techniques on F_o^2 (SHELXL-97 [25]). The program XP (Siemens Analytical X-Ray Instruments Inc., Madison, Wisconsin (USA)) was used for structure representations. Crystal data as well as details of data collection and refinement for the complexes are summarized in Table 4. Selected bond lengths (Å) and bond angles (deg) are listed in Table 2. Selected hydrogen bond lengths (Å) and angles (deg) are listed in Table 3.

Comments: The hydrogen atoms for **1a**, **2a**, **2b** and **3a** were placed in idealized geometrical positions. For **1a** and **2b** their isotropic displacement parameters were tied to the equivalent isotropic displacement parameters of the corresponding carrier atom by a factor of 1.2 or 1.5, while for **2a** and **3a** fixed displacement parameters were used. Anisotropic displacement parameters for **1a**, **2a**, **2b** and **3a** were applied to all non-disordered non-hydrogen atoms [25]. For **1a** disorder was observed for three of the *tert*-butyl groups. Two preferred orientations were refined resulting in site occupancies of 60(2) and 40(2) % for C30–C32 and C30A–C32A, of 85.9(8) and 14.1(8) % for C34–C36 and C34A–C36A, and of 63(2) and 37(2) % for C52–C54 and C52A–C54A. One of the PF_6^- anions is subjected to rotational disorder. Two preferred orientations were refined resulting in occupancies of 86.8(5) % for F21–F26 and 13.2(5) % for F21A–F26A. The compound crystallizes with a total of 2.5 molecules of acetone per formula unit. One of the acetone sites is only partially occupied (O200–C222, by approximately 50 %). A second acetone molecule is disordered with two alternative orientations of the C=O unit being occupied by 64(2) % for O200, C200 and 36(2) % for O210, C210. For the disordered structure parts a number of restraints were applied (SIMU, ISOR, SADI and SAME). The crystal structure of **2b** contains two sets of independent ions in the asymmetric unit. The two independent SO_4^{2-} anions are both disordered. Two orientations were refined that are occupied by 88.3(6) and 11.7(6) % for S1–O13 and S1A–O13A, and by 80.7(6) and 19.3(6) % for S2, O21, O24 and S2A, O21A, and O24A. SIMU restraints were applied in the refinement of this disorder. The compound crystallizes with a number of water molecules for which no hydrogen atoms were included in the structure model. The structure determination of **3** is of rather poor quality because the 2,2'-biimidazole ligand is superimposed by a bipyridine ligand.

CCDC 759063 (**1a**), 760286 (**2a**), 759064 (**2b**), and 760287 (**3a**) contain the supplementary crystallographic data (excluding structure factors) for this paper. These data can be obtained free of charge from The Cambridge Crystallographic Data Center via www.ccdc.cam.ac.uk/data_request/cif.

Reagents: Ruthenium trichloride, 2,2'-bipyridine and 4-methyl-1,2-phenylenediamine were of reagent grade and

used as supplied. [Ru(bpy)₂Cl₂] and [Ru(tbbpy)₂Cl₂] [11], tbbpy [26, 27], biimH₂ [28] and tmbibzimH₂ [29] were prepared according to literature procedures.

5,5'-Dimethyl-2,2'-bibenzimidazole

In a round bottom flask, 2.00 g (16.4 mmol) 4-methyl-1,2-phenylenediamine, 2.67 g (16.4 mmol) trichloroacetic acid and 20 mL of orthophosphoric acid were heated progressively to an end temperature of 180 °C. The condensation proceeded with the evolution of water and hydrogen chloride vapors. The resulting green-brown melt was hydrolyzed with 80 mL of water, and the off-white precipitate was filtered and neutralized with excess dilute ammonia. The free base was collected, thoroughly rinsed with water and dried to yield an off-white product. Yield: 1.5 g (91 %). – ¹H MMR (400 MHz, DMSO, r. t.): δ (ppm) = 7.28 (d, 2 H, H₇), 7.21 (s, 2 H, H₄), 6.60 (d, 2 H, H₆), 2.35 (s, 6 H, H_{Me}).

Bis-(4,4'-di(tert-butyl)-2,2'-bipyridine)-5,5',6,6'-tetramethyl-2,2'-bibenzimidazole-ruthenium(II) dichloride (**1**)

In a two-necked 250 mL round bottom flask, 91.0 mg (0.31 mmol) tetramethylbibenzimidazole (tmbibzimH₂) was suspended in 100 mL ethanol/water (ratio 4 : 1) and heated to 97 °C. Subsequently, 250 mg (0.35 mmol) [Ru(tbbpy)₂Cl₂] were dissolved in methanol and added dropwise to the suspension. The solution was refluxed over night whereupon the color changed to red. After cooling to r. t., the solvent was evaporated under reduced pressure. The residue was dissolved in acetonitrile and the resulting solution filtered. Acetonitrile was evaporated and the red solid dried *in vacuo*. Single crystals of **1a** suitable for X-ray crystallography were obtained by precipitation with ammonium hexafluorophosphate and subsequent slow evaporation of a solution of **1a** in acetone/pentane. Yield: 290 mg (82 %). – MS (FD in CH₂Cl₂, r. t.): *m/z* = 928 [M–2Cl]⁺. – ¹H MMR (270 MHz, CD₂Cl₂, r. t.): δ (ppm) = 8.41 (d, ⁴*J* = 1.84 Hz, 2 H, H_{tbbpy-3}), 8.33 (d, ⁴*J* = 1.76 Hz, 2 H, H_{tbbpy-3'}), 7.85 (d, ³*J* = 6.04 Hz, 2 H, H_{tbbpy-6}), 7.72 (d, ³*J* = 6.02 Hz, 2 H, H_{tbbpy-6'}), 7.48 (dd, ⁴*J* = 2.10 Hz, ³*J* = 6.02 Hz, 2 H, H_{tbbpy-5}), 7.48 (s, 2 H, H_{tmbibzimH2-G}), 7.25 (dd, ⁴*J* = 2.02 Hz, ³*J* = 6.06 Hz, 2 H, H_{tbbpy-5'}), 5.35 (s, 2 H, H_{tmbibzimH2-D}), 2.29 (s, 6 H, H_{tmbibzimH2-Me}), 2.00 (s, 6 H, H_{tmbibzimH2-Me'}), 1.49 (s, 18 H, H_{tbbpy-Me}), 1.37 (s, 18 H, H_{tbbpy-Me'}). – UV/Vis (H₂O): λ_{max} (ε_{max}) = 482 nm (8400 L mol⁻¹ cm⁻¹). Emission (H₂O): λ_{max} = 668 nm. Lifetime of excited state (H₂O): τ = 219 ns.

Bis-(4,4'-di(tert-butyl)-2,2'-bipyridine)-5,5',6,6'-tetramethyl-2,2'-bibenzimidazole-ruthenium(II) sulfate (**1b**)

Compound **1b** was synthesized according to **1**. The chloride salt was dissolved in water, and stoichiometric amounts

of sodium sulfate were added to precipitate **1b**. No crystals of **1b** suitable for structure determination could be obtained.

Bis-(2,2'-bipyridine)-5,5',6,6'-tetramethyl-2,2'-bibenzimidazole-ruthenium(II) dichloride (**2**)

In a two-necked 250 mL round bottom flask, 266 mg (0.91 mmol) tetramethylbibenzimidazole was suspended in 100 mL ethanol/water (ratio 4 : 1) and heated to 97 °C. Subsequently, 500 mg (1.03 mmol) [Ru(bpy)₂Cl₂] was dissolved in methanol and added dropwise to the suspension. The solution was refluxed over night while the color changed to red. After cooling to r. t., the solvent was evaporated under reduced pressure. The residue was dissolved in acetonitrile and the resulting solution filtered. Acetonitrile was exchanged by acetone, and a 0.1 M solution of sodium hydroxide was added until no further precipitation occurred. The resulting solid was separated and diluted with 0.1 M hydrochloric acid. The product was extracted three times with dichloromethane and the combined organic phases dried over sodium sulfate. Finally, the solvent was evaporated and the red solid dried *in vacuo*. Yield: 628 mg (79 %). – MS (ESI in methanol, r. t.): *m/z* = 703 [M–2Cl–H]⁺. – ¹H MMR (270 MHz, CD₂Cl₂, r. t.): δ (ppm) = 8.76 (d, ³*J* = 8.00 Hz, 2 H, H_{bpy-3}), 8.67 (d, ³*J* = 8.08 Hz, 2 H, H_{bpy-3'}), 8.16 (dt, ⁴*J* = 1.49 Hz, ³*J* = 7.98 Hz, ³*J* = 8.10 Hz, 2 H, H_{bpy-4}), 7.95 (m, 4 H, H_{bpy-6}, H_{bpy-4'}), 7.86 (d, ³*J* = 5.64 Hz, 2 H, H_{bpy-6'}), 7.48 (m, 4 H, H_{tmbibzimH2-G}, H_{bpy-5}), 7.27 (ddd, ⁴*J* = 1.20 Hz, ³*J* = 5.64 Hz, ³*J* = 7.39 Hz, 2 H, H_{bpy-5'}), 5.34 (s, 2 H, H_{tmbibzimH2-D}), 2.28 (s, 6 H, H_{tmbibzimH2-Me}), 1.99 (s, 6 H, H_{tmbibzimH2-Me'}). – ¹³C MMR (400 MHz, CD₂Cl₂, r. t.): δ (ppm) = 159.4, 157.5, 152.4, 152.1, 143.8, 140.2, 137.2, 136.8, 136.0, 134.3, 133.1, 127.5, 126.9, 124.5, 124.2, 114.9, 114.1, 20.4, 20.2. – UV/Vis (H₂O): λ_{max} (ε_{max}) = 472 nm (9300 L mol⁻¹ cm⁻¹). Emission (H₂O): λ_{max} = 654 nm. Lifetime of excited state (H₂O): τ = 95 ns.

Bis-(2,2'-bipyridine)-5,5',6,6'-tetramethyl-2,2'-bibenzimidazole-ruthenium(II) bis(hexafluorophosphate) (**2a**)

93.1 mg (0.19 mmol) [Ru(bpy)₂Cl₂] and 50.4 mg (0.19 mmol) 5,5'-dimethyl-2,2'-dimethylbibenzimidazole were suspended in 30 mL ethanol/water (ratio 2 : 1) and heated to reflux over night. The solution was cooled to r. t. and filtered. The volume of the filtrate was reduced to 10 mL, and a solution of 100 mg (0.61 mmol) ammonium hexafluorophosphate in 10 mL water was added to form a precipitate which was collected by filtration and washed twice with 10 mL water and diethyl ether. The crude product was purified by column chromatography on silica (THF/MeCN/sat. KNO₃ 12 : 4 : 0.5 v/v/v). Recrystallization from acetone/sat. NH₄PF₆ gave the pure product. Crystals suitable for

Table 4. Crystal structure data for **1a**, **2a**, **2b**, and **3a**.

| | 1a | 2a | 2b | 3a |
|--|---|--|--|--|
| Formula | C ₅₄ H ₆₆ N ₈ Ru (PF ₆) ₂ (C ₃ H ₆ O) _{2.5} | C ₃₆ H ₂₈ N ₈ Ru ₂ (PF ₆) (C ₃ H ₆ O) | C ₃₈ H ₃₄ N ₈ Ru (SO ₄)(H ₂ O) _{6.5} | C ₂₆ H ₂₂ N ₈ Ru(PF ₆) ₂ |
| <i>M_r</i> | 1363.35 | 1021.75 | 903.86 | 837.53 |
| Crystal size, mm ³ | 0.40 × 0.26 × 0.05 | 0.10 × 0.08 × 0.03 | 0.23 × 0.18 × 0.03 | 0.04 × 0.04 × 0.04 |
| Crystal system | triclinic | monoclinic | triclinic | trigonal |
| Space group | <i>P</i> $\bar{1}$ | <i>C</i> 2/ <i>c</i> | <i>P</i> $\bar{1}$ | <i>P</i> $\bar{3}$ <i>c</i> 1 |
| <i>a</i> , Å | 12.8555(8) | 18.0268(6) | 14.977(2) | 10.8215(9) |
| <i>b</i> , Å | 15.697(2) | 14.6071(4) | 15.395(2) | 10.8215(9) |
| <i>c</i> , Å | 18.050(2) | 16.2627(6) | 21.496(2) | 15.8621(15) |
| α , deg | 93.677(7) | 90 | 102.854(10) | 90 |
| β , deg | 95.678(5) | 93.101(1) | 110.251(9) | 90 |
| γ , deg | 113.399(6) | 90 | 95.862(9) | 120 |
| <i>V</i> , Å ³ | 3305.0(4) | 4276.0(2) | 4445.7(9) | 1608.7(2) |
| <i>Z</i> | 2 | 4 | 4 | 2 |
| <i>D</i> _{calcd} , g cm ⁻³ | 1.37 | 1.59 | 1.35 | 1.73 |
| μ (MoK α), mm ⁻¹ | 0.4 | 0.5 | 0.5 | 0.7 |
| <i>F</i> (000), e | 1416 | 2056 | 1848 | 832 |
| <i>hkl</i> range | ±15, ±19, ±22 | ±23, -17 → +18, ±21 | ±18, ±18, ±26 | ±12, ±12, ±18 |
| Refl. measured | 86622 | 8342 | 113826 | 10576 |
| Refl. unique | 12405 | 4886 | 16865 | 947 |
| <i>R</i> _{int} | 0.0853 | 0.0328 | 0.1579 | 0.0945 |
| Refl. observed [<i>F</i> _o ≥ 2 σ (<i>F</i>)] | 9808 | 3765 | 9799 | 727 |
| Param. refined | 963 | 281 | 1119 | 139 |
| <i>R</i> 1(<i>F</i>)/ <i>wR</i> 2(<i>F</i> ²) ^a [<i>F</i> _o ≥ 2 σ (<i>F</i>)] | 0.0694 / 0.1657 | 0.0591 / 0.1429 | 0.1021 / 0.2496 | 0.0649 / 0.1690 |
| <i>R</i> 1(<i>F</i>)/ <i>wR</i> 2(<i>F</i> ²) ^a (all refl.) | 0.0943 / 0.1787 | 0.0834 / 0.1540 | 0.1725 / 0.2811 | 0.169 / 0.1897 |
| <i>k</i> / <i>l</i> (weighting scheme) ^a | 0.001 / 24.248 | 0.080 / 5.744 | 0.100 / 0 | 0.121 / 2.773 |
| GoF (<i>F</i> ²) ^b | 1.132 | 1.253 | 1.543 | 1.078 |
| $\Delta\rho_{\text{fin}}$ (max / min), e Å ⁻³ | 1.27 / -0.73 | 1.66 / -0.89 | 2.78 / -0.80 | 2.18 / -0.67 |

^a $R1 = \sum |F_o - F_c| / \sum |F_o|$, $wR2 = [\sum w(F_o^2 - F_c^2)^2 / \sum w(F_o^2)^2]^{1/2}$, $w = [\sigma^2(F_o^2) + (kP)^2 + lP]^{-1}$, where $P = (\text{Max}(F_o^2, 0) + 2F_c^2) / 3$; ^b GoF = $[\sum w(F_o^2 - F_c^2)^2 / (n_{\text{obs}} - n_{\text{param}})]^{1/2}$, where n_{obs} is the number of data and n_{param} the number of refined parameters.

X-ray analysis were obtained from acetone/water. ¹H MMR investigations identified a statistical mixture of three possible isomers in a 1 : 2 : 1 ratio. A detailed analysis of the singlets at 5.40 and 5.38 ppm and the pseudo-triplet at 5.61 ppm, which are assigned to the bibenzimidazole arene protons (H_G) of all three possible isomers, confirmed this. Furthermore, the ratio of alkyl signals to aromatic signals is as expected.

Bis-(2,2'-bipyridine)-5,5',6,6'-tetramethylbi-2,2'-benzimidazole-ruthenium(II) sulfate (**2b**)

Compound **2b** was synthesized according to **2**. The chloride salt was dissolved in water and stoichiometric amounts of sodium sulfate were added to precipitate **2b**. Single crystals of **2b** suitable for structure determination were obtained upon covering a solution of **2** in ethanol/acetone with a small portion of a solution of sodium sulfate in water.

Bis-(2,2'-bipyridine)-2,2'-biimidazole-ruthenium(II) dichloride (**3**)

In a 250 mL round bottom flask, 40.3 mg (0.30 mmol) biimH₂ and 146.9 mg (0.30 mmol) [Ru(bpy)₂Cl₂] were suspended in 100 mL ethanol/water (ratio 4 : 1). The

solution was refluxed for 24 h whereupon its color changed to red. Afterwards, the solvent mixture was replaced by acetonitrile and filtered. Removing the solvent from the filtrate and subsequent drying *in vacuo* gave the pure red product. Crystals of **3a** suitable for X-ray structure determination were obtained by adding a small portion of ammonium hexafluorophosphate to a solution of **3** in water. Yield: 178.4 mg (95 %). – MS (ESI in methanol, r. t.): *m/z* = 546 [M–2Cl]⁺, 416 [M–2Cl–biimH₂+2H]⁺. – ¹H MMR (400 MHz, CD₃CN, r. t.): δ (ppm) = 8.45 (m, 4H, H_{bpy-3} and H_{bpy-3'}), 8.02–7.92 (m, 6H, H_{bpy-4}, H_{bpy-4'}, H_{bpy-6}/H_{bpy-6'}), 7.83 (m, 2H, H_{bpy-6'}/H_{bpy-6}), 7.44 (m, 2H, H_{bpy-5}/H_{bpy-5'}), 7.29 (m, 2H, H_{bpy-5'}/H_{bpy-5}), 7.26 (d, ³*J* = 1.2 Hz, 2H, H_{biimH2-D}), 6.38 (d, ³*J* = 1.2 Hz, 2H, H_{biimH2-E}). – ¹³C MMR (200 MHz, CD₃CN, r. t.): δ (ppm) = 159.4 (C_{bpy-2}/C_{bpy-2'}), 158.4 (C_{bpy-2'}/C_{bpy-2}), 153.4 (C_{bpy-6}/C_{bpy-6'}), 153.1 (C_{bpy-6'}/C_{bpy-6}), 141.6 (C_{biimH2-B}), 137.52 (C_{bpy-4}/C_{bpy-4'}), 137.45 (C_{bpy-4'}/C_{bpy-4}), 128.8 (C_{biimH2-D}), 128.2 (C_{bpy-5}/C_{bpy-5'}), 127.5 (C_{bpy-5'}/C_{bpy-5}), 124.5 (C_{bpy-3}/C_{bpy-3'}), 124.4 (C_{bpy-3'}/C_{bpy-3}), 121.2 (C_{biimH2-E}). – UV/Vis (H₂O): λ_{max} (ϵ_{max}) = 477 nm (9000 L mol⁻¹ cm⁻¹). Emission (H₂O): λ_{max} = 650 nm.

Acknowledgements

N.R. acknowledges the German Environmental Foundation (DBU) for financial support. S. R. and D.M. G. acknowledges financial support from the DFG and the Collaborative Research Center 583.

-
- [1] V. Balzani, F. Scandola, *Supramolecular Photochemistry*, Ellis Horwood, Chichester, **1991**.
- [2] N. C. Fletcher, P. C. Junk, D. A. Reitsma, F. R. Keene, *J. Chem. Soc., Dalton Trans.* **1998**, 133–138.
- [3] S. Serroni, G. Denti, S. Campagna, A. Juris, M. Ciano, V. Balzani, *Angew. Chem.* **1992**, *104*, 1540–1542; *Angew. Chem., Int. Ed. Engl.* **1992**, *31*, 1493–1495.
- [4] A. J. Downard, G. E. Honey, L. F. Phillips, P. J. Steel, *Inorg. Chem.* **1991**, *30*, 2259–2260.
- [5] P. Majumdar, S.-M. Peng, S. Goswami, *J. Chem. Soc., Dalton Trans.* **1998**, 1569–1574.
- [6] Y. Cui, Y.-L. Niu, M.-L. Cao, K. Wang, H.-J. Mo, Y.-R. Zhong, B.-H. Ye, *Inorg. Chem.* **2008**, *47*, 5616–5624.
- [7] S. Rau, L. Böttcher, S. Schebesta, M. Stollenz, H. Görls, D. Walther, *Eur. J. Inorg. Chem.* **2002**, 2800–2809.
- [8] S. Rau, B. Schäfer, S. Schebesta, A. Grüßing, W. Popitz, D. Walther, M. Duati, W. R. Browne, J. G. Vos, *Eur. J. Inorg. Chem.* **2003**, 1503–1506.
- [9] M. Haga, *Inorg. Chim. Acta* **1983**, *45*, L183–L184.
- [10] M. Haga, *Inorg. Chim. Acta* **1983**, *75*, 29–35.
- [11] S. Rau, B. Schäfer, A. Grüßing, S. Schebesta, K. Lamm, J. Vieth, H. Görls, D. Walther, M. Rudolph, U. W. Grummt, E. Birkner, *Inorg. Chim. Acta* **2004**, *357*, 4496–4503.
- [12] M. Gottschaldt, U. S. Schubert, S. Rau, S. Yano, J. G. Vos, T. Kroll, J. Clement, I. Hilger, *Chem. Bio. Chem.* **2010**, DOI 10.1002/cbic.200900769, in press.
- [13] D. Walther, L. Böttcher, J. Blumhoff, S. Schebesta, H. Görls, K. Schmuck, S. Rau, M. Rudolph, *Eur. J. Inorg. Chem.* **2006**, 2385–2392.
- [14] S. Rau, M. Ruben, T. Büttner, C. Temme, S. Dautz, H. Görls, M. Rudolph, D. Walther, A. Brodkorb, M. Duati, C. O'Connor, J. G. Vos, *J. Chem. Soc., Dalton Trans.* **2000**, 3649–3657.
- [15] S. Rau, T. Büttner, C. Temme, M. Ruben, H. Görls, D. Walther, M. Duati, S. Fanni, J. G. Vos, *Inorg. Chem.* **2000**, *39*, 1621–1624.
- [16] A. M. Bond, M. Haga, *Inorg. Chem.* **1986**, *25*, 4507–4514.
- [17] D. P. Rillema, R. Sahai, P. Matthews, A. K. Edwards, R. J. Shaver, L. Morgan, *Inorg. Chem.* **1990**, *29*, 167–175.
- [18] R. Taylor, O. Kennard, W. Versichel, *Acta Crystallogr.* **1984**, *B40*, 280–288.
- [19] A. Bondi, *J. Phys. Chem.* **1968**, *68*, 441–451.
- [20] SADABS (version 2.06), Bruker Analytical X-Ray Instruments Inc., Madison, Wisconsin (USA) **2002**.
- [21] R. Hooft, COLLECT, Nonius KappaCCD Data Collection Software, Nonius BV, Delft (The Netherlands) **1998**.
- [22] DENZO-SMN, Z. Otwinowski, W. Minor, in *Methods in Enzymology*, Vol. 276, *Macromolecular Crystallography*, Part A (Eds.: C. W. Carter, Jr., R. M. Sweet), Academic Press, New York, **1997**, p. 307.
- [23] G. M. Sheldrick, SHELXTL NT (version 6.12), Bruker Analytical X-Ray Instruments Inc., Madison, Wisconsin (USA) **2002**.
- [24] G. M. Sheldrick, *Acta Crystallogr.* **1990**, *A46*, 467–473.
- [25] G. M. Sheldrick, SHELXL-97 (release 97-2), Program for the Refinement of Crystal Structures, University of Göttingen, Göttingen (Germany) **1997**. See also: G. M. Sheldrick, *Acta Crystallogr.* **2008**, *A64*, 112–122.
- [26] T. B. Hadda, H. Le Bozec, *Polyhedron* **1988**, *7*, 575–577.
- [27] P. Belser, A. von Zelewsky, *Helv. Chim. Acta* **1980**, *63*, 1675–1702.
- [28] E. E. Bernarducci, P. K. Bharadwaj, R. A. Lalancette, K. Krogh-Jespersen, J. A. Potenza, H. J. Schugar, *Inorg. Chem.* **1983**, *22*, 3911–3920.
- [29] E. Müller, G. Bernardinelli, J. Reedijk, *Inorg. Chem.* **1995**, *34*, 5979–5988.